Materials Science-Poland, *Vol. 28*, *No. 3*, *2010*

Synthesis of mesoporous silica by cationic surfactant templating in various inorganic acid sources

W.-D. XIANG[1], Y.-X. YANG[2, 3*], J.-L. ZHENG[2], L. CAO[2], H.-J. DING[2], X.-N. LIU[4]

[1]College of Chemistry and Materials Engineering, Wenzhou University, Wenzhou, Zhejiang 325035, P.R. China

[2]Department of Chemistry, East China University of Science and Technology, 200237, P.R.China

[3]State Key Laboratory of Inorganic Synthesis and Preparative Chemistry, College of Chemistry, Jilin University, Changchun 130012, P.R. China

[4]Analysis Test Center, Yangzhou University, Yangzhou, 225009, P.R.China

Mesoporous silica materials with well-ordered hexagonal structure were synthesized under acidic conditions. The influences of crystallization conditions, aging conditions, acid sources HX and acid/ tetraethyl orthosilicate ratio on the order degree and the morphology have been discussed. The increase of crystallization temperature or crystallization time was beneficial for the condensation of silica species, but had no effect on improving the order degree of mesoporous silica. The order degree of mesoporous materials using various acid sources HX under the same acid concentration swas as follows: HNO_3＞HBr＞ H_2SO_4＞HCl which differed from that in the Hofmeister series; the sulfate anions SO_4^{2-} can play a supporting role on pore structure in the form of space occupation, leading to forming more ordered products than in HCl. Besides, the NO_3^- and Br^- ions showed contrary effect on the growth of micelles, the bigger the pore wall thickness we obtained, the less HBr or the more HNO_3 we used.

Keywords: *mesoporous silica; synthesis conditions; acid source; acidic anions*

1. Introduction

Since the publication by Mobil's scientists,of the first paper on the so-called M41S family of mesoporous molecular sieves with regularly ordered mesopore arrangements and narrow pore size distributions, mesoporous materials have attracted increasing attention due to growing interest in their engineering applications as well as

*Corresponding author, e-mail: yxyang@ecust.edu.cn

in heterogeneous catalysis, ion exchange, adsorption separation and other advanced techniques. So far, various synthetic routes have been developed, including S^+I^-（S^-I^+, $S^+X^-I^+$, $S^-M^+I^-$, SI, NI, etc. [1–4]. Among them, the synthetic routes of well-ordered hexagonal mesoporous silica belong to the S^+I^- and $S^+X^-I^+$ pathways. According to Huo [3] et al., the alkaline route involves direct co-condensation of anionic inorganic species with a cationic surfactant in the S^+I^- pathway. By contrast, the acid route involves condensation of ionic inorganic species in the presence of similarly charged surfactant molecules, this $S^+X^-I^+$ pathway is mediated by counterions of opposite charge to that of the surfactant head group.

It is noted that the synthesis by the S^+I^- route is different from that by the $S^+X^-I^+$ route. As Huo et al. pointed out, the S^+I^- route is carried out in alkaline conditions by self-assembly of anionic silicates and cationic surfactant molecules [3], where $S^+ = C_nH_{3n+1}N^+(CH_3)_3$, n = 8–18, and I^- is the anionic silicate species. The synthesis is performed under conventional hydrothermal conditions, which usually requires that the reaction system be under a liquid self-pressure, and at high temperature for a long reaction time. This will restrict the engineering applications of mesoporous materials.

However, the $S^+X^-I^+$ route achieves self-assembly via a different route from the former, but it uses the same long quaternary ammonium surfactant as a structure-directing agent in acid condition, where $S^+ = C_nH_{3n+1}N^+(CH_3)_3$, $X^- = Cl^-$, Br^-, SO_4^{2-}, NO_3^-, etc., I^+ is a cationic silicate species. As Stucky et al. proposed [5], the ammonium surfactant S^+ is used as a templating agent, but the acid anion X^- plays a role in this route, as it serves to buffer the repulsion between the I^+ and the S^+ by means of weak hydrogen bonding forces in acidic conditions. Thus the $S^+X^-I^+$ route can offer more versatile structures and morphologies than the S^+I^- route, due to its weaker surfactant/silicate interaction in $S^+X^-I^+$, the association of S^+X^- determines the structure and morphology of the mesoporous materials.

It is noted that the acidic system has the pH value lower than 2, the soluble silicate species promote acidic ionization, because their isoelectric point (IEP) is larger than 2 [6, 7]. Thus the mesoporous materials framework is considered as formation via the $S^+X^-I^+$ self-assembly route in acidic media [3]. The advantage of this method is that the reaction system needs no liquid self-pressure, and the high quality mesoporous molecular sieves can be obtained by a reaction of short duration at low temperature.

Although hexagonal close-packing mesoporous silica can be obtained either in alkaline conditions or in acidic conditions, there are lots of differences in both properties such as the pore size, pore wall thickness and pore structure, except that they have the similar crystal symmetry. Stucky [5] proposed that acid synthesis and alkaline synthesis are two different routes via a quite different internal mechansim. At present, less attention is focused on studies of acid synthesis, in contrast to studies of alkaline synthesis. In particular, there have been few comprehensive studies on the conditions of syntheses. Thus in this paper, we discuss experimental factors affecting acid synthesis, including acid sources, the molar ratio of acid/ tetraethyl orthosilicate (TEOS), the temperature and the reaction time, in order to study the influence of various experi-

mental conditions on the order degree and properties of mesoporous materials. Here, we find that ordered mesoporous silica can be synthesized, using a surfactant etyltrimethylammonium bromide (CTAB) templating in a acid medium, by the $S^+X^-I^+$ route at a low temperature of 30 °C, and in a short time ca. 24 h. We attempted to obtain highly ordered mesoporous materials, based on the results of comprehensive tests on various acidic anions.

2. Experimental

Reagents. The following reagents were used: cetyltrimethylammonium bromide (CTAB), nitric acid, hydrochloric acid, hydrobromic acid, and sulfuric acid (all A.R. grade, Shanghai Chemical Reagent Company Ltd., China), tetraethyl orthosilicate (TEOS, Shanghai Chemical Reagent Company Ltd., China).

Synthesis of mesoporous silica. The structure directing agent CTAB was dissolved in HBr(aq.), HCl(aq.), HNO_3(aq.), H_2SO_4(aq.) respectively, with vigorous stirring, followed by slowly adding TEOS in certain proportions. The chemical composition of the mother gel was 1 CTAB : 3.0 TEOS : 18.7 HX : 741 H_2O, where X : Cl^-, NO_3^-, SO_4^{2-}, or Br^-. The resulting mixture was stirred at 30–35 °C and kept static to aging. Then it was cooled down to room temperature (RT). The resulting white precipitate was filtered, washed with deionized water and dried in air at RT. Finally, the product was calcined at 550 °C for 6 h; the temperature was raised from RT to 550 °C under the heating rate of 2 °C·min^{-1}.

Characterization. The powder X-ray diffraction measurements of the mesoporous silica were performed on a D/max 2550 VB/PC X-ray diffractometer, using Ni-filtered CuK_α radiation (40 mA, 40 kV, 1° (2θ) min^{-1}) at RT. The Fourier transform infrared (FTIR) spectrum was recorded on a Nicolet 510P FT-infrared spectrometer, over the spectral range of 4000–400 cm^{-1}, at the resolution of 2 cm^{-1}, using KBr wafers.

The pore images and ordering of mesoporous silica were observed with a JEOL JEM-2100F type transmission electron microscope, operated at 200 kV. The surface morphology of mesoporous silica was observed with a Hitachi s4800 field emission scanning electron microscope, at an accelerating voltage of 15.0 kV. The samples were dispersed in ethanol by sonication and subsequently dropped on carbon microgrids.

Nitrogen adsorption–desorption measurements at 77.4 K were carried out on an ASAP2405 volumetric adsorption analyzer from Micromeritics. Before the measurements, the samples of mesoporous silica were outgassed at 600 °C in the adsorption apparatus, the surface area of the mesoporous silica was calculated, using the BET equation, from adsorption data within the P/P_0 range of 0.05–0.30. The adsorption capability and pore structure of calcined mesoporous silica were calculated from the adsorption isotherms, by the BJH approach.

3. Results and discussion

3.1. Analysis of the experimental process

After a few seconds, when TEOS was slowly added to the acid solution in the presence of CTAB, ivory-white colloidal precipitate was produced which indicates that the TEOS had been hydrolyzed SiO_2 gel formed. The longer the stirring time, the greater the quantity of precipitate produced.

The process has been conducted in two stages: the first stage begins with the TEOS addition and ends when the precipitation process is complete; the second stage starts with the crystallization process and ends with the aging process. During the first stage, a magnetic stirrer must be used for stirring, while during aging process, in the second stage, the sample should be kept static at constant temperature. It was also found that CTAB did not easily dissolve in HBr(aq.), unlike the other three acids.

3.2. The role of crystallization temperature and crystallization time on the mesoporous synthesis

As Huo et al. proposed, well-ordered hexagonal mesoporous silica could be synthesized at room temperature in the acidic medium [3, 7]. It is questionable, however, whether this temperature is optimum with respect to the ordering and properties of mesoporous silica. How will the quality of mesoporous silica be influenced by an increase in the temperature? To answer this question, subsequent discussion shall be based on the results of experimental tests.

Figure 1 shows small angle X-ray powder diffraction (SXRD) patterns of the products synthesized, using HCl and HBr as the acid sources, at various temperatures. The SXRD pattern for the as-made product synthesized using HCl by crystallization at 30 °C shows one strong (100) diffraction peak, $2\theta = 2.14°$, and two weak diffraction peaks, $2\theta = 3.64°$ and $4.24°$ (Fig. 1), which are indexed to the (110) and (200) crystal faces, respectively. The corresponding crystal plane spacing d_{100} was calculated to be 4.12 nm, based on the Bragg formula $\lambda = 2d\sin\theta$. This shows that the sample is strongly representative of a hexagonal symmetry channel structure. The results of indexing of the SXRD pattern with $a = 4.1440$ nm $c = 2.7911$ nm are given in Table 1. HCl was the acid source at 30 °C, the XRD data refer to the as-synthesized sample. d_{exp} is the empirical value for the interplanar spacing, and d_{cal} is the theoretical value of the interplanar spacing, *hkl* are the Miller indices for the hexagonal unit cell. Table 1 shows that all the diffraction peaks in the pattern of the as-made product can be readily indexed by a set of lattice parameters. The largest relative deviation between the theoretical predictions and the experimental data is 0.23%, which indicates that the as-made product, synthesized by crystallization at 30 °C, is a single phase with hexagonal symmetry.

The SXRD patterns for the as-made product synthesized by crystallization at 50 °C and 70 °C all show a strong (100) diffraction peak near 2.52°, corresponding to

the crystal plane spacing of about 3.50 nm; it is evident however that the (100) diffraction peak has been broadened to some extent, and that the (110) diffraction peak is hard to distinguish. For the product crystallized at 90 °C, a poor SXRD pattern was observed, which exhibits a broadening peak with a peak packet near 2.00° in the low-angle region, indicating that the product contains large amount of non-hexagonal phase, and thus the (100) diffraction peak was heavily widened.

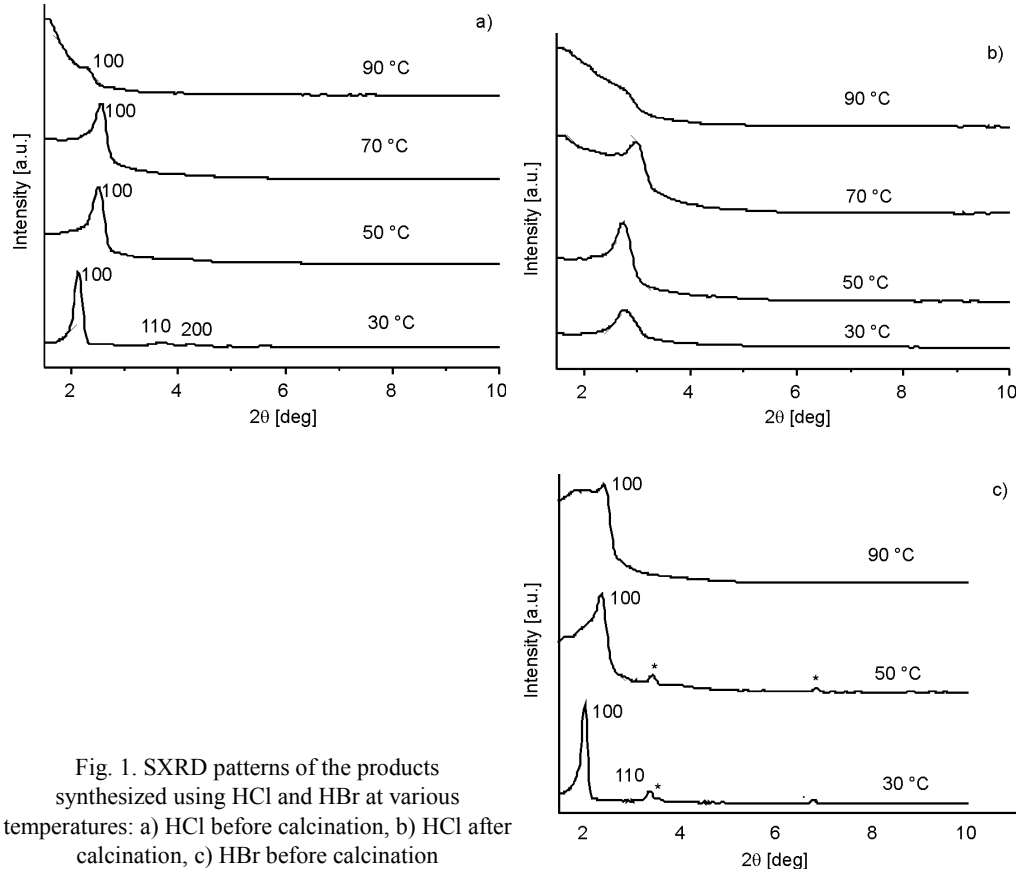

Fig. 1. SXRD patterns of the products synthesized using HCl and HBr at various temperatures: a) HCl before calcination, b) HCl after calcination, c) HBr before calcination

Table 1. The index results of XRD data

2θ [deg]	d_{exp} [nm]	d_{cal} [m]	*hkl*
2.14	4.1249	4.1440	100
3.64	2.4253	2.3925	110
4.26	2.0725	2.0720	200

As a note, according to our analysis presented above, when the crystallization temperature increases from 30 °C to 90 °C and when HCl as the sole source of acid, the crystallization degree of the as-made products obviously becomes lowered, and the pore arrangements of the as-made products become more disordered. By comparing

SXRD patterns of the products synthesized using HCl before and after calcination, as shown in Fig. 1, it can be observed that the peak shape of each calcined product becomes less sharp than that of the as-made product, indicating that the ordering degree decreases. It is probably because a large amount of template is removed after calcination, leading to the inorganic framework collapsing to a different extent.

As can be seen in Fig. 1, the SXRD pattern for the as-made product synthesized using HBr by crystallization at 30 °C shows one strong (100) diffraction peak, $2\theta = 2.02°$, corresponding to a crystal plane spacing of 4.37 nm; and two weak diffraction peaks at $2\theta = 3.52°$ and 4.08°, which are indexed to the (110) and (200) crystal faces, respectively. It is consistent with the reported data regarding the characteristic diffraction peak of MCM-41, and it indicates that an inorganic framework of as-made products is obtained and has a hexagonal mesoporous structure. Furthermore, two undefined weak peaks appear; they are labeled by stars at about 3.40° and 6.70° within the range of $2\theta = 3–7°$. For clarity, an XRD experiment was also performed on CTAB. The results showed two well-defined strong diffraction peaks at about 3.40° and 6.70°, which indicates that the two aforementioned, poorly defined, weak diffraction peaks can be attributed to CTAB. Because of the poor solubility of long hydrophobic chains CTAB in HBr(aq.). the unreacted template separates out during the formation of mesoporous silica.

When the crystallization temperature rises to 50 °C, the as-made product displays one defined (100) diffraction peak at 2.37°, and two peaks of template CTAB, but the peak corresponding to (110) crystal faces is hard to distinguish. One can also observe an apparent broadening of the (100) peak with a peak packet in the low-angle region, when the crystallization temperature reaches 90 °C, indicating the as-made product has a low degree of crystallization. Thus it may be concluded from Fig. 1 that upon increasing the crystallization temperature, the degree of crystallinity and pore order of as-made products becomes lower, if HBr is the sole acid source.

Thus, no matter what source of acid we use, the degree of crystallinity and pore order of the as-made products both decrease upon increasing the crystallization temperature. It is probably because there is an aggregation-dissociation balance between template agent micelles and individual template agent molecules in the synthesis system [7]. When the temperature increases, the molecule thermal movements are accelerated, the molecules of template in micelles are easy to free itself from bound states, and become individual molecules. It leads to the number of micelles decreasing.

In addition, the higher thermal activity of molecules causes instabilities among the micelles, and thus the packing arrangements of micelles become less ordered. When the product is crystallized at 50 °C and 70 °C, the density of the micelles decreases, and the packing arrangements of micelles become slightly disordered. For this reason, the condensation rate of silica species also increases. It leads to the formation of many high polymers of silicon species, even the formation of some amorphous substances among sparse micelles. As a consequence, the SXRD patterns of the as-made product crystallized at 50 °C and 70 °C are broader and less defined than that of the product crystallized at 30 °C.

When the product is crystallized at 90 °C, the packing arrangements of micelles become relatively disordered; the density of micelles in solution obviously decreases as well but the condensation rate of silica species seriously increases. This leads to the formation of quite a large number of amorphous silica among sparse micelles, and thus the SXRD patterns become broader and less distinct, resulting in broadening of the (100) diffraction peak. Consequently, an increase in the crystallization temperature can accelerate the condensation rate of inorganic species, if synthesis is performed in an acid aqueous medium, but it makes no improvement to the quality of the products. On the contrary, it probably causes degradation in the quality of the product.

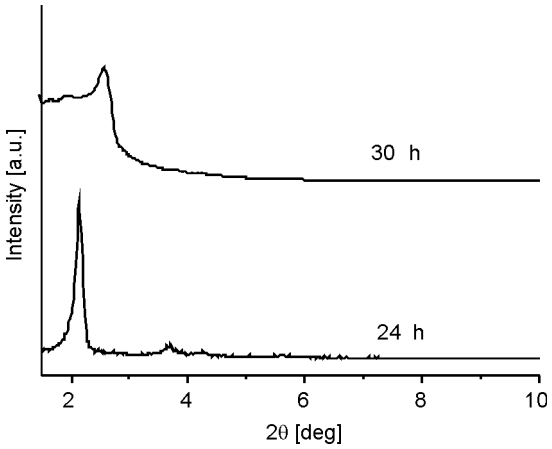

Fig. 2. SXRD patterns of the samples synthesized at various time

Figure 2 shows SXRD patterns of the products synthesized at 30 °C using HCl as the acid source for various durations of crystallization. When the as-made product is crystallized for 24 h, the SXRD pattern displays a well-defined diffraction peak and two weak diffraction peaks in the range of 1.0–10°. Whereas the as-made product is crystallized for 30 h, the SXRD pattern displays a single broadening peak indexed as (100) diffraction, which indicates low order of the product. This demonstrates that a prolonged crystallization time results in a poor degree of crystallinity and low-ordered pore structure of as-made products. It is probably because prolonged crystallization time leads to the deterioration of the mesopore structure [8], and disappearance of the mesoporous features. According to Gao [9], the crystal product may change into amorphous state after prolonged crystallization. This is also noted that the MCM-41 phase is in a metastable state, prolonged crystallization time may cause the system to transform into more stable amorphous state.

3.3. Role of aging temperature and aging time in the mesoporous synthesis

Figure 3 shows SXRD patterns of the products at various aging temperatures with various aging times after crystallization at 50 °C for 30 h, using HBr as the sole source

of acid. It can be seen from Fig. 3 that at comparatively low temperatures (50 °C or 30 °C), no matter how the two factors, aging temperature or prolonging the aging time are changed, the peak profiles in the SXRD patterns can be observed to remain almost unchanged. This indicates the above two factors have no influence on the degree of crystallinity or on the ordering of the pore structure of the products. Because the hexagonal structure of the products has been formed after crystallization for a certain time, so low aging temperature has no effect on the stability of hexagonal arrays of cylindrical micelles, and prolonging the aging time has no significant effect on the degree of crystallinity and ordering of pore structure. This demonstrates that under the precondition of keeping no effect on the stability of the micelles, the ordered hexagonal structure may not be influenced by the condensation of the silicate species.

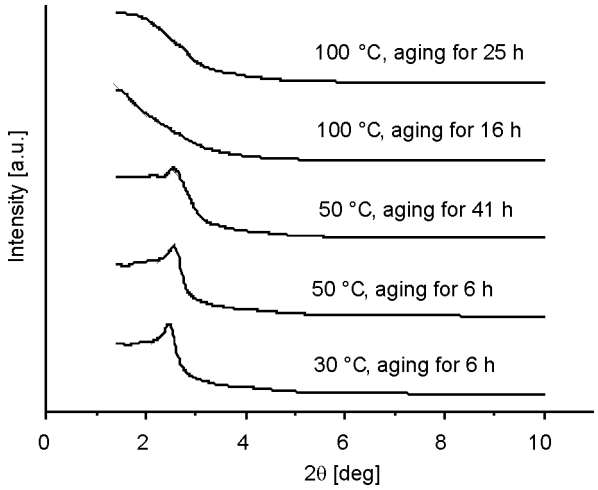

Fig. 3. SXRD patterns of the samples synthesized under various aging conditions

When the crystallized product was transferred to the hydrothermal reactor for aging at 100 °C, the degree of crystallinity and the ordering of the pore structure decreased sharply. As shown in Fig. 3, after aging at 100 °C for 16 h or 25 h, its diffraction peaks in the low-angle region disappeared completely. It occurs because the stability of loose hexagonal arrays of cylindrical micelles may be influenced by a high aging temperature, while the condensation and deposition of silicate species are accelerated if the aging temperature is raised, thereby leading to the decrement of both the degree of crystallinity and the ordering of the pore structure. The results described above demonstrate that the reaction temperature should be limited to 100 °C in acid synthesis, otherwise the order and quality of the mesoporous product will be seriously degraded. This route is different from alkaline synthesis, in which most products are synthesized at temperatures above 100 °C. In the case of alkaline synthesis, high temperatures can feasibly accelerate the condensation of silicate species in the crystallized product, and optimize the degree of long range order. However, in the case of acid

synthesis, such is not the case. In conclusion, high temperature alkaline synthesis is feasible, whereas high temperature acid synthesis is not feasible.

3.4. Acid source with various acidic anions

To study the influence of acidic anions for four various acid sources on the order and quality of the mesoporous product, the mesoporous materials were synthesized by using CTAB as the surfactant and TEOS as a silica source in the presence of various acid sources: H_2SO_4, HCl, HBr, and HNO_3.

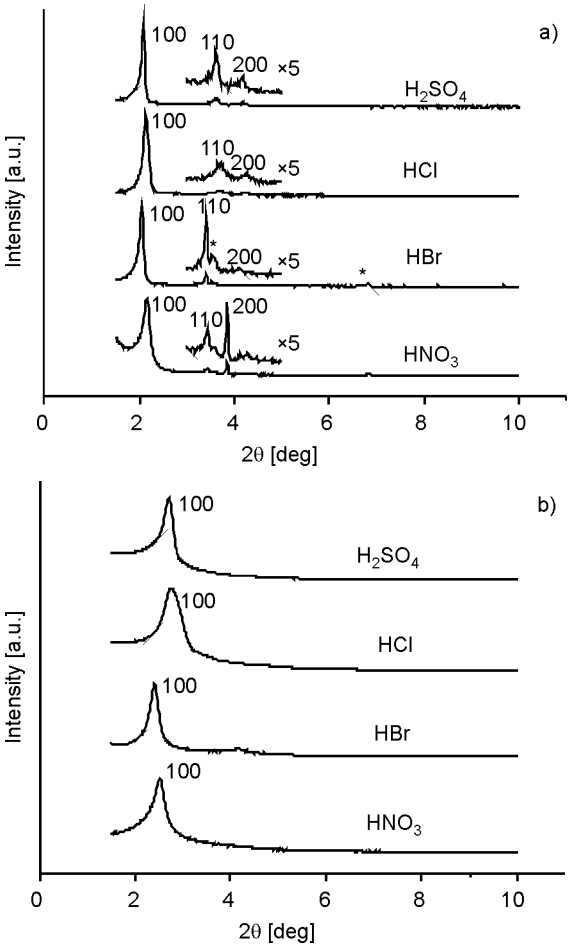

Fig. 4. SXRD patterns of the samples synthesized using various acid sources: a) before calcination (the illustration is locally magnified), b) after calcination

Figure 4 shows the SXRD patterns of the crystallized product at 30 °C before and after calcination. It was found that the synthesis using HBr acid leads to the appearing

a diffraction peak of the template (denoted with the asterisk in Fig. 4a). That is due to poor solubility of the template CTAB in HBr (aq.). Even when CTAB was dissolved in HBr (aq.) under stirring for a long time, there were still some white deposits in the solution, so that a small quantity of undissolved template was mixed with the as-made products. As can be seen from Fig. 4a, all the SXRD patterns of the as-made products display a strong well-defined (100) diffraction peak, and several medium-sized or small peaks in the range of 3–5°, indicating the inorganic framework of the as-made products, which is typical for a hexagonally symmetric channel structure of mesoporous MCM-41.

The order degree of mesoporous materials can be measured from the peak intensity and the half-peak width in low-angle diffraction. As shown in Fig. 4a, when HNO_3 is used as the acid source, the SXRD pattern of the as-made product exhibits a strong, well-defined (100) diffraction peak, and two medium-sized peaks in the range of 3–5°. If HBr is used as the acid source, the resulting product material exhibits a medium-sized peak and a small peak in the range of 3–5°, which are both less intense than those corresponding to HNO_3. If H_2SO_4 is the acid source, a medium peak and a small one are observed beside one strong diffraction peak, showing the low mesoporous order of the product, compared with the HBr sample. However, using HCl acid results in two small peaks in the range of 3–5°, as compared to three products using HNO_3, HBr and HCl. Therefore, the order degree of the mesoporous materials is observed to decrease in the following order: $HNO_3 > HBr > H_2SO_4 > HCl$, which points to unusual anion response, different from the so-called Hofmeister series (from most ordered to least ordered): $NO_3^- > Br^- > Cl^- \sim SO_4^{2-}$ [10].

According to Huo et al. [3, 7], the chief driving force governing self-assembly in an acidic medium is an electrostatic interaction between the positive charged silicon species (I^+) and the cationic micelles (S^+X^-) with the attached counterions (X^-), which can catalyze the condensation of positive-charged silicon species. The higher is the constant of association of counterions with a cationic surfactant, the stronger the association between the (S^+X^-) micelles and the silicon species (I^+), and thus more stable micelles are formed, leading to the formation of more ordered products.

As reported by Lin, at 30 °C the association constants of NO_3^-, Br^- and Cl^- on the CTAB micelles are 0.220, 0.122 and 0.018 respectively [11]. Based on these results, we can conclude that the order degree of our products decreases in the following order: $HNO_3 > HBr > HCl$. It is reasonable and consistent with the above analysis. Unlike three different monovalent anions, the sulfate anions SO_4^{2-}, simple tetrahedral oxoanions, can adopt a number of coordination modes, such as monodentate, bidentate bridging, bidentate chelating, tridentate, and even tetradentate bridging, etc., contributing to the structural diversities of the final networks [12]. In contrary to Cl^- anions, they can act as ligands to form hydrogen bonds with the micelle S^-N^+ and silicates species I^- in several ways, and thus promote growth and stability of micelles, leading to forming more ordered products than those fabricated using HCl.

Figure 4b shows the SXRD pattern of the calcined products by using various acid sources HX (HCl, HBr, HNO_3, H_2SO_4). One can clearly observe that nearly all these products possess one main diffraction peak at (100) crystal face, except the product obtained using HCl. It shows more broadening than the corresponding peak for the as-made product. It probably occurs because a large number of templates are removed when the products are calcined, causing the pore wall of the product obtained with HCl to collapse. Another explanation for the peak-broadening might be asymmetrical condensation of the residual silicon species, resulting from the presence of Cl^- anions and high temperature calcination.

In synthesis, when each initial reactant mole ratio was fixed, the products that had been synthesized using various acid sources had rather rich morphologies. Thus, we can use SEM to compare and study these different morphologies.

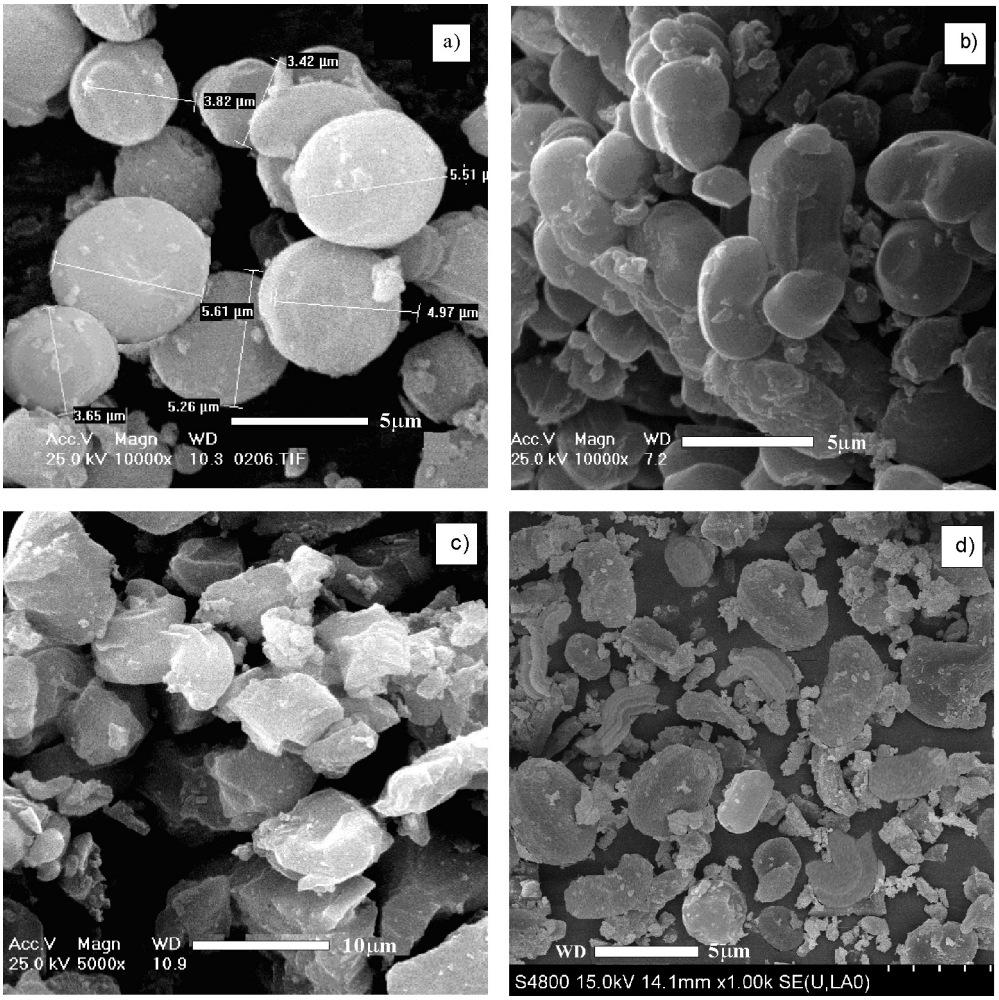

Fig. 5. SEM of the samples synthesized using various acid sources a) HNO_3 b) HBr c) HCl d) H_2SO_4

As we can see from the SEM images shown in Fig. 5, the surface curvature of the products decreased in the following order: $NO_3^- > Br^- > SO_4^{2-} > Cl^-$. For HNO_3, the resulting product consisted of micrometer-sized gyroidal spheres. When HBr was used as the acid source, the product was observed to consist of cashew-like particles. When HCl was used as the acid source, the resulting product appeared the least ordered among all the products obtained with an acid source; Figure 5c shows a disordered block-like structure. When the acid source was H_2SO_4, the resulting product appeared less ordered than the two products obtained with HNO_3 and HBr. The images of the product derived with H_2SO_4 are shown in Fig. 5d: they exhibit a mixture of spherical, ellipsoidal and caterpillar-like shapes of various sizes and non-uniform distributions.

So far, the formation mechanism of incredible morphologies has not been clarified yet, but it is certain that all these morphologies discussed above maybe related to the formation process of interior ordered mesostructures which can be controlled by acidic anionic ions [13]. The following anions are listed in increasing order of their ionic radii: $NO_3^- < Br^- < Cl^- < SO_4^{2-}$. Acidic anions having smaller ionic radii make more associations between the surfactants and the silicates, compared with those having larger anionic radii, so more charges are neutralized, ultimately leading to a more ordered morphology [14].

With HNO_3 as the acid source, NO_3^- ions have the smallest ionic radii among four anionic ions used in the experiment. Therefore, the association of NO_3^- between surfactants and silicates is strongest. The largest amount of charges neutralized would in turn help the formation of gyroidal spheres. By careful observations, we also find that spiral distortion occurs on the surface of the spherical shapes, as shown in Fig. 5a. Maybe because large steric hindrance during the process of micelle formation of NO_3^- induces strong space repulsion between adjacent two layers of micelles, spiral distortion helps to reduce the repulsive effect.

With HCl as the acid source, Cl^- ions have relatively large ionic radii, leading to weak association of Cl^- between surfactants and silicates, and thus less of charge neutralized. As a result, the micelle surface has large charges left, and the lower surface curvature cause the formation of disordered, block-like structures.

According to existing literature, NO_3^- and Br^- anions have stronger binding strength to the surfactant, in comparison with SO_4^{2-} and Cl^- anions. However, the ionic radius of Br^- lies between the ionic radii of NO_3^- and Cl^-. Therefore, during the process of association with surfactants and silicates, the surface charges are partly neutralized, which determines the formation of a cashew-like morphology.

With H_2SO_4 as the acid source, the divalent SO_4^{2-} anions adsorbed on the pore wall preferentially bind with free hydroxyl ions of mesoporous silica. This effectively reduces the number of free hydroxyl ions on the pore wall, and thus prevents the pore structure from collapsing as a result of bonding and dehydration of free hydroxyls. And to certain degree, it also plays a role of structure direction agent. Simultaneously,

space occupation of SO_4^{2-} can play a supporting role on pore structure in several ways due to its different coordination modes, leading to formation of mixture of spherical, ellipsoidal and caterpillar-like structures.

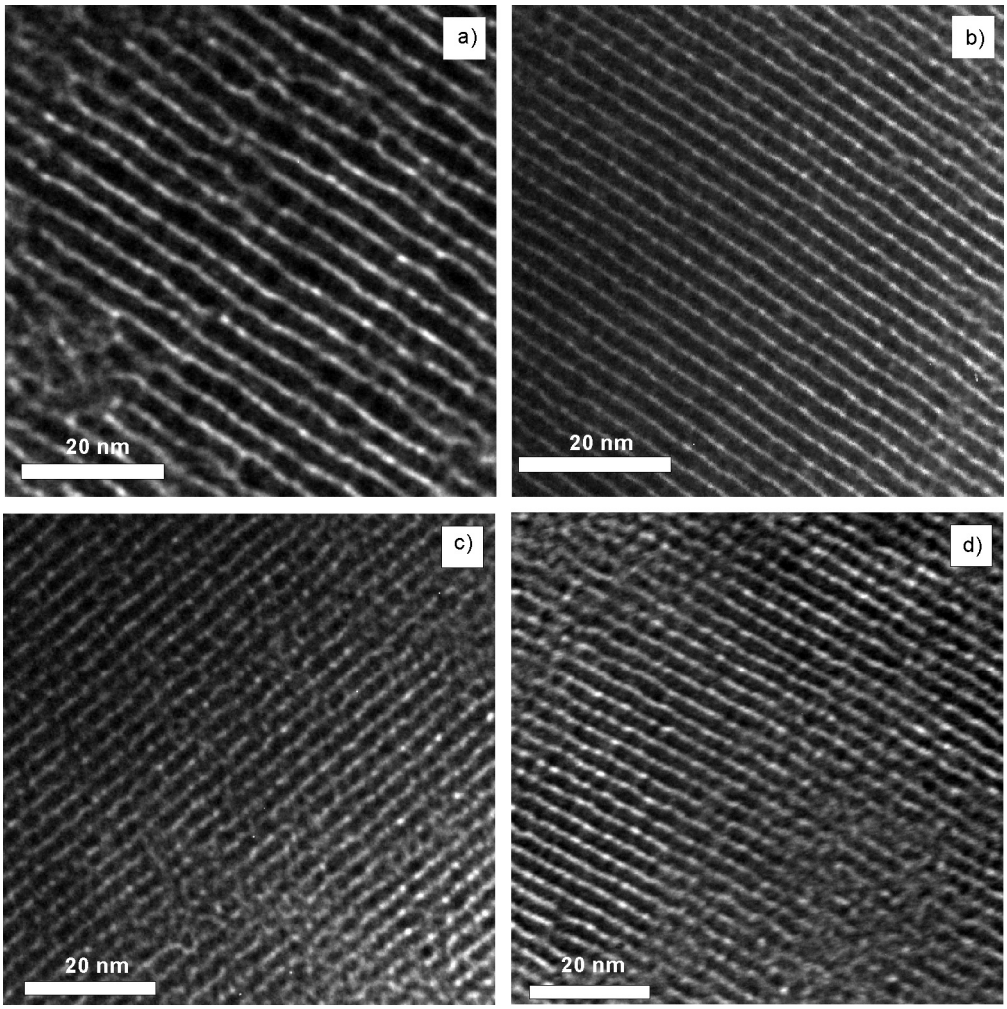

Fig. 6. TEM of the products synthesized using various acid sources a) HNO_3 b) HBr c) HCl d) H_2SO_4

Figures 6a and 6b show that with HNO_3 and HBr, the resulting products all have hexagonal structures. The TEM image shown in Fig. 6 clearly illustrates an ordered arranged pore channel structure with a bend or kink. In the top right hand corner of Fig. 6a, a non-parallel pore channel with kink helices can be observed, which may lead to the formation of micrometer sized gyroidal spheres, shown in Fig. 5a. When HBr is the acid source, the product exhibits a well ordered parallel oriented pore channel structure can be observed along the [110] direction, as the image shown in Fig. 6b

the image clearly shows a large number of hexagonal structure channels and packing along the axis of parallel channel. In a word, the products synthesized with HNO_3 and HBr both present regularly, well-ordered parallel arranged pore channel structure. It is because the strong association interaction between NO_3^-, Br^- and cationic surfactant that favors the stability of the micelles forming.

As shown in Fig. 6c, the TEM image of the product with HCl shows only discontinuous pore channels, indicating low order degree of these samples. But when using H_2SO_4 as acid sources, an ordered parallel pore channel can be seen in Fig. 6d, except for a part of discontinuous channels shown in the lower right corner. It thus leads to a conclusion that the order degree of our products decreases as follows: $HNO_3 > HBr > H_2SO_4 > HCl$, in a good agreement with the conclusion based on XRD and SEM analyses.

To investigate the effect of the acid source on the pore size of the products and the shrinkage of cells in the product after calcination, nitrogen adsorption–desorption measurements at 77.4 K were carried out on an ASAP2405 volumetric adsorption analyzer from Micromeritics. The adsorption capability and pore structure of calcined mesoporous silica were calculated from the adsorption isotherms obtained by the BJH method.

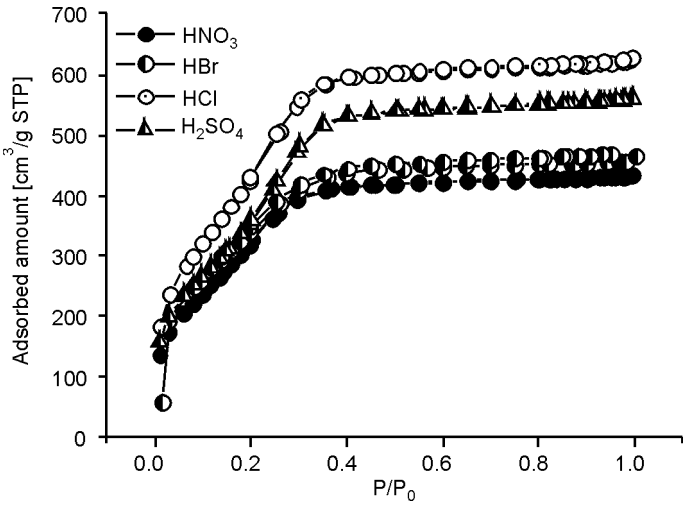

Fig. 7. Sorption isotherms of the products synthesized using various acid sources

In Figures 7 and 8, N_2 sorption isotherms of the products are shown, using various acid sources, all belonging to standard type IV at the relative pressure P/P_0 of 0.01–0.99, showing the presence of mesopores. The measured Brunauer–Emmett –Teller surface areas (S_{BET}) of the products derived with HNO_3, HBr, HCl and H_2SO_4 as acid sources are 1297, 1309, 1661 and 1466 m^2g^-, respectively. Their pore volumes (V_p) are 0.9021, 0.6901, 0.9598 and 0.8571 $cm^3 \cdot g^{-1}$, respectively.

The physisorption isotherm of the products derived with HNO_3, HBr, H_2SO_4 and HCl all show hysteresis loops. The two branches in the isotherm remain nearly horizontal and parallel over a wide range of relative pressures between 0.30 and near saturation, indicating inkbottle type mesopores. Rapid change in the amount of N_2 sorption causes only minor variation in the corresponding relative pressure, indicating a relatively narrow distribution of pore sizes in the three products.

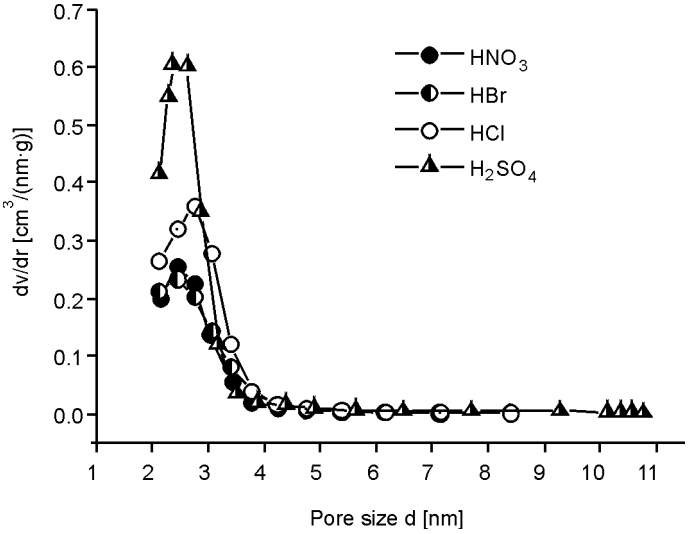

Fig. 8. Pore size distributions of the products synthesized using various acid sources

As can be seen in Fig. 7, the capillary condensation occurred in the pore channel of product with HNO_3, HBr, H_2SO_4 and HCl was located at various middle parts of adsorption isotherms, the location of them moved from low to high values of P/P_0 in the incremental order: $HNO_3 \approx HBr < H_2SO_4 < HCl$, so the product derived with HCl showed a large hysteresis loop at high P/P_0, which is generally indicative of a large pore size.

As can be seen in Fig. 8, the product derived with H_2SO_4 exhibits the strongest peak among all products derived from the four considered acid sources. The product derived with HCl shows a stronger peak than for the products derived with HNO_3 or HBr, near the 2.70 nm radius. This indicates that the product derived with H_2SO_4 has the highest percentage of small pores, and that the product derived with HCl, and the second highest percentage small pores. The percentages of pores of most probable sizes in the products with HNO_3 and HBr were calculated about 71.3% and 68.4% respectively, while the percentage in products with HCl and H_2SO_4 were calculated about 85.6% and 91.6%, respectively.

It was also found that the pore diameter of the product derived with HCl is 2.74 nm, thus it is larger than the pore diameters of the products derived with other

acids, namely 2.44 nm, in the case of HNO_3 and HBr, and 2.52 nm for the product derived with H_2SO_4.

Thus it can be seen that the pore sizes and pore volumes of synthesized products are different for various acid sources. The detailed parameters of pore structure measured by N_2 sorption-desorption isotherms are given in Table 2, where D is the pore size, L – pore wall thickness ($L = a_0 - D$), a_0 – the unit cell constant ($a_0 = 2d_{100}/3^{1/2}$), d_{100} is the interplanar spacing of the synthesized products after calcination. The Δd_{100} value shows shrinkage of a cell after calcination due to template removal and silicon species polycondensation in the pore wall. When polycondensation degree of silicon species is low in mesoporous material formation, a looser pore wall tends to be formed, and thus results in a larger Δd_{100} value.

Table 2. Porous properties of synthesized products on pore size, surface area and pore wall thickness with various acid source

Product identifier	Before calcination		After calcination		$\Delta d100$ [nm]	a_0 [nm]	S_{BET} [m^2/g]	V_P [cm^3/g]	D [nm]	L [nm]
	2θ [deg]	d_{100} [nm]	2θ [deg]	d_{100} [nm]						
HNO_3	2.142	4.121	2.487	3.549	0.572	4.098	1297	0.9022	2.440	1.658
HBr	2.018	4.374	2.413	3.658	0.716	4.224	1309	0.6901	2.440	1.784
HCl	2.119	4.166	2.786	3.169	0.997	3.659	1661	0.9598	2.740	0.919
H_2SO_4	2.096	4.211	2.684	3.289	0.922	3.798	1466	0.8571	2.523	1.275

Basically, we find that all of these mesoporous materials exhibit large surface areas (ca. 1300 m^2/g) and uniform pore sizes. Furthermore, the pore sizes can be adjusted by changing the acid source used in the synthesis. The d spacings vary with the choice of the acid source; by comparing the decrement in the d_{100} value after calcination at 550 °C, one can observe that the decrement, (Δd_{100}), in the d_{100} value for the HNO_3 product is only about 0.572 nm smaller than the corresponding decrements for the other acids (about 1.0 nm). While the pore wall thickness (L) for the HNO_3 product appears to be large, as presented in Table 2, it indicates that the strongly adsorbed NO_3^- ion catalyzes more effectively condensation of silicon species and facilitates the formation of a stronger wall for the hexagonal structure in mesoporous silica. It was also found that Δd_{100} for the HBr product is about 0.716 nm smaller than for HCl and H_2SO_4 ones, indicating that the negative species Br^- binds more strongly to the surfactant than either Cl^- or HSO_4^-. The Δd_{100} for the HCl product shows the largest value, yet the pore wall thickness of the HCl product apparently decreases, further demonstrating that Cl^- binds the most weakly to the surfacant.

The parameter Δd_{100} of the H_2SO_4 product is slightly lower than for the HCl product. The pore wall thickness for the H_2SO_4 product appears to be larger than for the HCl product. This indicates a stronger binding of the negative species SO_4^{2-} to the

surfactant, compared with the binding of Cl^- to the surfactant, and it is in very good agreement with the SXRD results.

In order to study the coordination properties of SO_4^{2-} and Cl^- anions to the silicate species I^-, we also performed IR experiments on the products made with HCl and with H_2SO_4. The spectra of these two as-made products are shown in Fig. 9.

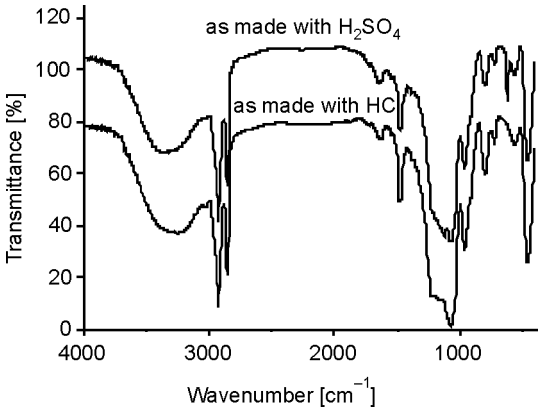

Fig. 9. Infrared spectrum of two as-made products

The IR spectra of the two as-made products are relatively similar and broad bands corresponding to stretching vibration of the Si–OH group at 3371 cm^{-1} and sharp bands to asymmetric Si–O–Si stretching vibrations at 1073 cm^{-1} occur in both spectra. The symmetric Si–O–Si stretching vibrations occur at 801 cm^{-1}, whereas the Si–O–Si bending modes at 458 cm^{-1}. Thus, the IR spectra indicate that the products must be the silica.

As can be seen in Fig. 9, the two as-made products also display two distinct peaks corresponding to CH_2 and CH_3 groups of CTAB at 2930 cm^{-1} and 2852 cm^{-1}, and to three stretching vibrations of CH_2 at 1633 cm^{-1}, 1482 cm^{-1} and 728 cm^{-1}. Also, a weak band at 564 cm^{-1} can be attributed to the Br^- of CTAB, indicating the presence of surfacant in the as-made product. In contrast to the IR spectra of the as-made product with HCl, the as-made product with H_2SO_4 also displays two weak bands of SO_4^{2-} occurring at 1129 cm^{-1} and 620 cm^{-1}, which illustrates that SO_4^{2-} acidic anions were actually involved in a templated self-assembly process of mesoporous material. But there is no evidence of Cl^- bands in Fig. 9; perhaps this is because only a very small number of Cl^- acidic anions participated in the actual formation of the mesoporous material, a number so small that their presence is not detectable by the infrared sensor. The results demonstrate that SO_4^{2-} acidic anions show stronger binding to the as-made product than the Cl^- acidic anions.

According to Huo and Yokoi et al. [3, 15], quaternary cationic surfactants CTAB can associate the acidic anions (X^-) to form S^+X^- micelles in an acidic environment, which can catalyze the condensation of the positive-charged cationic silicate species

(I^+). Thus the mesostructure formation of S^+X^-–I^+ mesoporous intermediates is driven by the electrostatic interaction of the positive-charged silicate species (I^+) and micelle association of the S^+X^- in this paper. The divalent anions SO_4^{2-} can act as ligands, to form hydrogen bonds with the micelle S^+ as well as the silicates species I^+, which perhaps enhances the interaction between I^+ and S^+X^-. However, the Cl^- anions as negative counter-ions, are different from the SO_4^{2-} anions; they have a shielding effect for the positive charge on the S^+ micelle surface due to the polarizability of Cl^- anions [16]. This causes the strength in counter-ion binding of Cl^- to S^+ micelles less than that in counter-ion binding of SO_4^{2-} to S^+ micelles. On the other hand, the anions SO_4^{2-}, as negative counterions, also have a shielding effect for the positive charge on the S^+ micelle surface [17], leading to weaker binding of the negative species SO_4^{2-} to surfactant than that of NO_3^- and Br^- to surfactant. Now, this leads to conclusion that the series orders ions with increasing the strength in counter-ion binding to micelles of CTAB from left to right under the same acid concentration, and is as follows: Cl^-, SO_4^{2-}, Br^-, NO_3^-, instead of so-called Hofmeister series orders SO_4^{2-}, Cl^-, Br^-, NO_3^-.

Next, we investigated the influence of various acid contents on the products. We studied the acid systems HNO_3 and HBr for they all have the strongest binding tendency. At a HA/TEOS molar ratio between 1 and 3, the influence of acid contents is more apparent. The N_2 adsorption studies were performed with the same instrumentation to investigate the influence of the acid content on pore size of the products.

3.5. Role of acid contents

As can be seen from Figs. 10 and 11, the crystallinity degree and structure ordering of two products using HA (HNO_3, HBr) all increase as the molar ratio of HA to TEOS ranges from 1 to 3 in the low-angle region, which is in accordance with the report of Zhang et al [18]. In this study, we also found that increase of the HNO_3 content resulted in an enlargement of the *d* spacing of the X-ray d_{100} peak. This enlargement corresponds to the two strong peaks, related by hexagonal symmetry, which appear in the SXRD pattern. But incremental addition of HBr content resulted in a decrease in *d* spacing of the X-ray d_{100} peak, whereas low HBr content resulted in an apparent broadening (100) peak with a peak packet in a low-angle region. This is because various anions in HA can interact with TEOS to modify the rates of hydrolysis and particle nucleation, affecting the final particle size and the extent of cationic silicate species condensation in the materials, leading to different properties of surfaces and morphologies of the final products [19].

Nnitrate anions possess a higher charge density than bromide anions [10] and they also are characterized by π electronic structure, forming hydrogen bonds with the micelle S^-N^+ and silicon species I^- by bidentate bridging [16]. Consequently they can reduce the repulsion between the surfactant headgroups, and thus affect contraction of

micelle in solution. This leads to decreasing radii of micelles as the HA/TEOS ratio increases. However, bromide anions, as heavier halogen ions, show correspondingly stronger π back-donation [20, 21], they can form the d-pπ back-donation, accepting the electron from nitrogen element in the $(CH_3)_3\overset{+}{N}-$ groups of micelle S^-N^+, which makes the surfactant headgroups more positive. This may produce more repulsive force between head groups, and thus affects expandability of micelle in solution, leading to radius of micelle increasing as HA/TEOS ratio increases. The results shown in Tables 3 and 4 can confirm these conclusions.

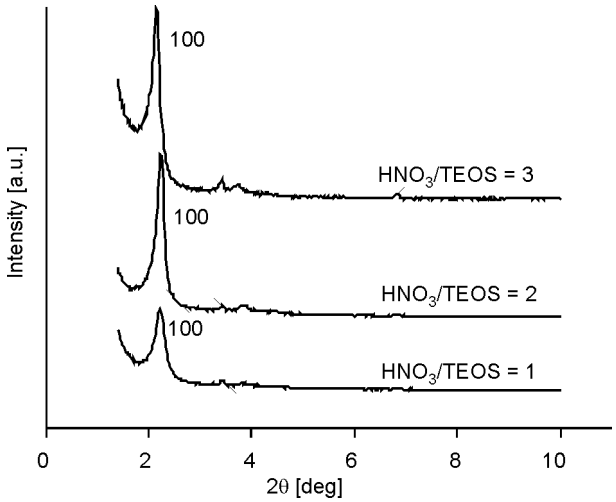

Fig. 10. SXRD patterns of the samples with HNO_3 at various HA/TEOS ratios

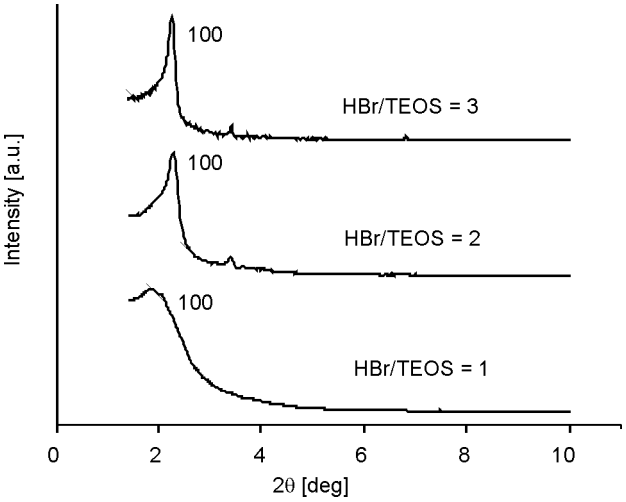

Fig. 11. SXRD patterns of the samples with HBr at various HA/TEOS ratios

Table 3. Porous properties of the samples with HNO_3 at various HA/TEOS ratio

HNO_3 /TEOS	Before calcination		After calcination		Δd_{100} [nm]	a_0 [nm]	S_{BET} [m^2/g]	V_P [cm^3/g]	D* [nm]	L* [nm]
	2θ [deg]	d_{100} [nm]	2θ [deg]	d_{100} [nm]						
3	2.141	4.123	2.514	3.511	0.612	4.054	1691	0.9297	2.555	1.499
2	2.210	3.994	2.560	3.448	0.546	3.981	1782	0.9410	2.493	1.488
1	2.278	3.875	2.611	3.381	0.494	3.904	1316	0.7462	2.820	1.084

Table 4. Porous properties of the samples with HBr at various HA/TEOS ratio

HNO_3 /TEOS	Before calcination		After calcination		Δd_{100} [nm]	a_0 [nm]	S_{BET} [m^2/g]	V_P [cm^3/g]	D [nm]	L [nm]
	2θ [deg]	d_{100} [nm]	2θ [deg]	d_{100} [nm]						
3	2.266	3.896	2.588	3.411	0.485	3.939	1119	0.7950	2.693	1.125
2	2.263	3.901	2.514	3.511	0.390	4.054	1388	0.7275	2.456	1.598
1	1.838	4.802	1.979	4.460	0.342	5.150	1302	0.7224	2.507	2.643

By comparing the decrement of the d_{100} value (Δd_{100}) of the product before and after calcination in Tables 3 and 4, one may conclude that its value does not depend on the acid type but only on the acid content. Because the decrease of the unit cell before and after calcination is originated from condensation of silicate species in pore wall, thus the higher the condensation degree of the product before calcination, the more compact the pore wall is, and thus the lower the value of Δd_{100}. It leads to conclusion that decreased acid content favours the condensation of the inorganic species. As is known, in the acid synthesis system, the acidic medium plays a dual role. It not only promotes the hydrolysis of TEOS, and protonation of oligomeric silicate species but also produces anions of X^- in the surface layer of the electrical double layer structure. For these reasons, when the acid content is decreased, the electric charge density of oligomeric silicate species decreases, leading to static electric repulsion decreasing between the silicate species. This favors crosslinking and condensation between them, resulting in a compact pore wall, and a decrease of Δd_{100}. On the other hand, a decrease of concentration of anions of the electrical double ayer structure can decrease drive force of the silicate species aligning along template micelles, and this goes against assembly of organic-inorganic interface. In short, the two factors make self-condensation rate of inorganic species apparently higher than the assembly rate along the template surface, thus this results in a considerable amount of SiO_2 high polymer producing among the assembled template micelles, even the amorphous products being formed. Consequently, the quality and the ordering degree of the product decrease inevitably.

4. Conclusion

Increase of the crystallization temperature and the crystallization time are beneficial for the condensation of silica species, but have no effect on improving the order of products in acid conditions. The order degree of mesoporous materials with various acids is as follows: $HNO_3 > HBr > H_2SO_4 > HCl$, which seems to be different from the Hofmeister series NO_3^-, Br–, Cl–, SO_4^{2-}. The products consist of micrometer sized gyroidal spheres, cashew like, and disordered block like structures, corresponding to the products derived with HNO_3, HBr, and HCl. However, SO_4^{2-} anions can enhance the pore structure in several modes, leading to the formation of a product which consists of a mixture of spherical, ellipsoidal and caterpillar like structures. Various acid contents are another key factor affecting the order and pore size of products. With increasing acid contents, the ordering of products increases, but the pore size of product with HNO_3 decreases, while with HBr increases accordingly.

Acknowledgements

The authors are grateful for the financial support provided by the National Natural Science Foundation of China (Grants Nos. 20971043, 50772075), the Open Project Program of State Key Laboratory of Inorganic Synthesis and Preparative Chemistry, Jilin University.

References

[1] KRESGE C.T., LEONOWICZ M.E., ROTH W.J., VARTULI J.C., BECK J.S., Nature, 359 (1992), 710.
[2] BECK J.S., VARTULI J.C., ROTH W.J., LEONOWICZ M.E., KRESGE C.T., SCHMITT K.D., CHU C.T.W., OLSON D.H., SHEPPARD E.W., J. Am. Chem. Soc., 114 (1992), 10834.
[3] HUO Q., MARGOLESE D.I., CIESLA U., FENG P., GIER T.E., SIEGER P., LEON R., PETROFF P.M., SCHFITH F., STUCKY G.D., Nature, 368 (1994), 317.
[4] TANEV P.T., PINNAVAIA T.J., Science, 267 (1995), 865.
[5] HUO Q., MARGOLESE D.I., CIESLA U., DEMUTH D.G., FENG P., GIER T.E., CHMELKA B.F., SCHUTH F., STUCKY G.D., Chem. Mater., 6 (1994), 1176.
[6] ILER R.K., *The Chemistry of Silica*, Wiley, New York, 1979, pp. 489, 644, 651, 674.
[7] YANG Y., ZHANG J., YANG W., WU J., CHEN R., Appl. Surf. Sci., 206 (2003), 20.
[8] GAO X.H., MAO X.W., TANG R.R., ZHANG Y.M., SHEN S.K., Acta Petrolei Sinica (Petroleum processing section), 14 (1998), 17.
[9] WANG J., VINU A., COPPENS M.-O., J. Mater. Chem., 17 (2007), 4265.
[10] LEONTIDIS E., Curr. Opinion Coll. Inter. Sci., 7 (2002), 81.
[11] LIN H.P., KAO C.P., MOU C.Y., LIU S.B., J. Phys. Chem. B, 104 (2000), 7885.
[12] SUNA Y.-Q., YANG G.-YU, Dalton Trans., 34 (2007), 3771.
[13] LIN H.P., MOU C.Y., Accounts Chem. Res., 35 (2002), 927.
[14] XU R.R., PAN W.Q., *Chemistry. Zeolites and Porous Materials*, Science Press, 2004, p. 614.
[15] YOKOI T., YOSHITAKE H., YAMADA T., KUBOTA Y., TATSUMI T., J. Mater. Chem., 16 (2006), 1125.
[16] YANG Y.-X., HUANG Z., DENG W.-J., SHAO J.-G., CHEN Y.-R., LIU X.-N., Microp. Mesopor. Mater., 116 (2008), 267.
[17] YANG Y.-X., ZHANG J.-B., LIU X.-N., CHEN Y.-R., JIA X.-C., J. Amer. Ceram. Soc., 90 (2007), 2050.
[18] ZHANG Z.R., SUO J.S., ZHANG X.M., LI S.B., Acta Phys.-Chim. Sin., 14 (1998), 243.

[19] PALMQVIST A.E.C., Curr. Op. Coll. Int. Sci., 8 (2003), 145.
[20] GREENWOOD N.N., EARNSHAW A., *Chemistry of the Elements*, 2nd Ed., Butterworth-Heinemann, Jordan Hill, Oxford, 1984, pp. 195–196.
[21] MIESSLER G.L., TARR D.A., *Inorganic Chemistry*, 3rd Ed., Pearson, Prentice Hall, Upper Saddle River, NJ, 1991, pp. 154–157.

Received 20 January 2010
Revised 16 September 2010